AD-A161 239 THE VARIATION IN THE SUBGRAIN SIZE IN ALUMINUM DEFORMED 1/1
TO LARGE STEADY-STATE CREEP STRAINS(U) NAVAL
POSTGRADUATE SCHOOL MONTEREY CA P P MIESZCZANSKI
UNCLASSIFIED SEP 85 F/G 11/6 NL

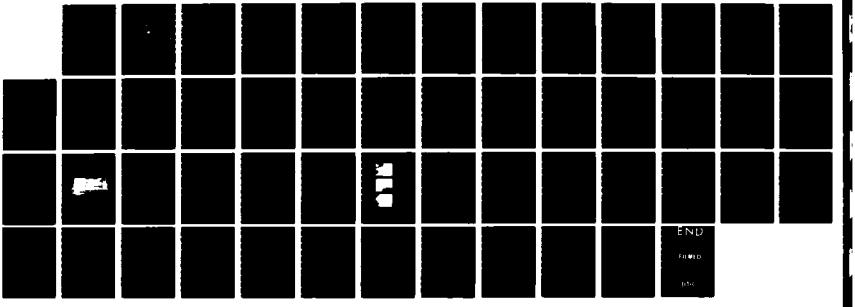

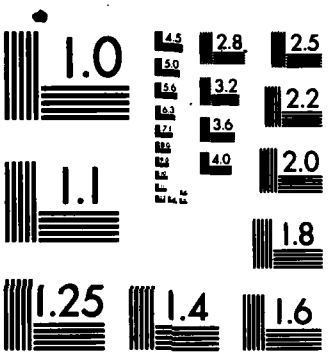

MICROCOPY RESOLUTION TEST CHART
NATIONAL BUREAU OF STANDARDS-1963-A

NAVAL POSTGRADUATE SCHOOL
Monterey, California

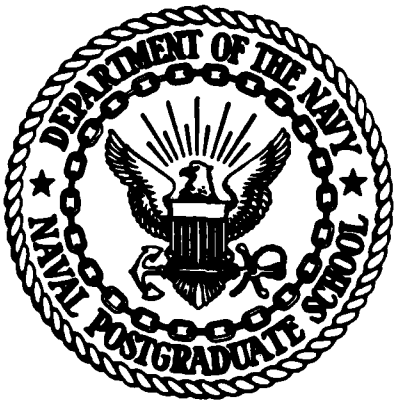

THESIS

THE VARIATION IN THE SUBGRAIN SIZE
IN ALUMINUM DEFORMED TO LARGE
STEADY-STATE CREEP STRAINS

by

Paul P. Mieszczanski

September 1985

Thesis Advisor: M. E. Kassner

Approved for public release; distribution is unlimited

SECURITY CLASSIFICATION OF THIS PAGE (When Data Entered)

REPORT DOCUMENTATION PAGE		READ INSTRUCTIONS BEFORE COMPLETING FORM
1. REPORT NUMBER	2. GOVT ACCESSION NO.	3. RECIPIENT'S CATALOG NUMBER
4. TITLE (and Subtitle) THE VARIATION IN THE SUBGRAIN SIZE IN ALUMINUM DEFORMED TO LARGE STEADY-STATE CREEP STRAINS		5. TYPE OF REPORT & PERIOD COVERED Master's Thesis; September 1985 6. PERFORMING ORG. REPORT NUMBER
7. AUTHOR(s) Paul P. Mieszczanski		8. CONTRACT OR GRANT NUMBER(s)
9. PERFORMING ORGANIZATION NAME AND ADDRESS Naval Postgraduate School Monterey, California 93943-5100		10. PROGRAM ELEMENT, PROJECT, TASK AREA & WORK UNIT NUMBERS
11. CONTROLLING OFFICE NAME AND ADDRESS Naval Postgraduate School Monterey, California 93943-5100		12. REPORT DATE September 1985 13. NUMBER OF PAGES 50
14. MONITORING AGENCY NAME & ADDRESS(if different from Controlling Office)		15. SECURITY CLASS. (of this report) Unclassified 15a. DECLASSIFICATION/DOWNGRADING SCHEDULE

16. DISTRIBUTION STATEMENT (of this Report)

Approved for public release; distribution is unlimited

17. DISTRIBUTION STATEMENT (of the abstract entered in Block 20, if different from Report)

18. SUPPLEMENTARY NOTES

19. KEY WORDS (Continue on reverse side if necessary and identify by block number)

Superplasticity, Aluminum, Creep, Torsion Testing, Subgrain Size, Forest Dislocation Density, Misorientation Angle, Dislocation Separation Distance, Low Angle Dislocation Boundary

20. ABSTRACT (Continue on reverse side if necessary and identify by block number)

Pure metals (and many alloys) deformed at high (creep) temperatures strain-harden. This hardening is associated with an increase in the density of randomly arranged (forest) dislocations and subsequent formation of a three-dimensional network of low-angle dislocation boundaries (subgrains). Eventually a material reaches a steady-state condition, and hardening and recovery processes are balanced. A controversy

DD FORM 1 JAN 73 1473 EDITION OF 1 NOV 65 IS OBSOLETE

S N 0102-LF-014-6601

SECURITY CLASSIFICATION OF THIS PAGE (When Data Entered)

20. (Continued)

exists as to which of these features is primarily responsible for creep resistance or strength. During steady-state deformation, the feature responsible for creep strength is expected to be invariant with strain. Some stainless steel work suggested that the subgrain size changes during steady-state. Therefore, it was believed that subgrain strengthening is not dominant in this material. Aluminum specimens were deformed to various large steady-state strains and examined by transmission electron microscopy to determine the average subgrain size. It was found that the subgrain size was constant over a very wide ($\varepsilon \approx 16$) range of steady-state strain.

Approved for public release; distribution is unlimited

The Variation in the Subgrain Size in Aluminum Deformed to Large Steady-State Creep Strains

by

Paul P. Mieszczanski
Lieutenant, United States Navy
B.S., Fairfield University, 1976

Submitted in partial fulfillment of the
requirements for the degree of

MASTER OF SCIENCE IN MECHANICAL ENGINEERING

from the

NAVAL POSTGRADUATE SCHOOL
September 1985

Author: Paul P. Mieszczanski
Paul P. Mieszczanski

Approved by: M. E. Kassner
M. E. Kassner, Thesis Advisor

P. J. Marto
P. J. Marto, Chairman, Department
of Mechanical Engineering

John M. Dyer
John N. Dyer, Dean of Science and Engineering

ABSTRACT

Pure metals (and many alloys) deformed at high (creep) temperatures strain-harden. This hardening is associated with an increase in the density of randomly arranged (forest) dislocations and subsequent formation of a three-dimensional network of low-angle dislocation boundaries (subgrains). Eventually a material reaches a steady-state condition, and hardening and recovery processes are balanced. A controversy exists as to which of these features is primarily responsible for creep resistance or strength. During steady-state deformation, the feature responsible for creep strength is expected to be invariant with strain. Some stainless steel work suggested that the subgrain size changes during steady-state. Therefore, it was believed that subgrain strengthening is not dominant in this material. Aluminum specimens were deformed to various large steady-state strains and examined by transmission electron microscopy to determine the average subgrain size. It was found that the subgrain size was constant over a very wide ($\epsilon = 16$) range of steady-state strain.

TABLE OF CONTENTS

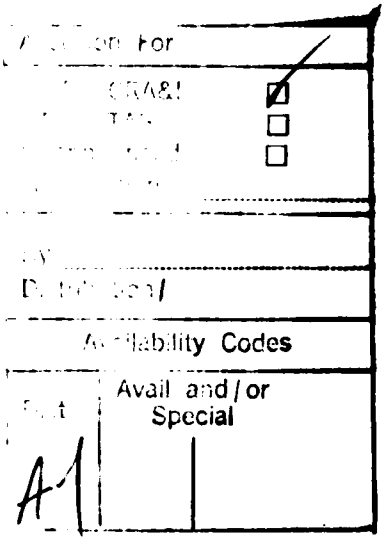

LIST OF FIGURES

ACKNOWLEDGEMENT

I would like to thank my advisor, Professor M. E. Kassner, for his knowledgeable guidance during all phases of the research. Thanks are also extended to Dr. E. W. Lee, Dr. P. Deb, Dr. Adachi, and T. Kellogg for their assistance in metallography, microscopy, and micrograph developing and printing.

I. INTRODUCTION

A. RESEARCH IMPORTANCE

Material resistance to plastic deformation at high temperatures has become an important consideration for turbine, chemical, petrochemical, and nuclear industries. In particular, there is a need to understand and predict material response to complicated thermal-mechanical history. The purpose of this research was to identify the important microstructural features associated with the elevated temperature strength in high-purity aluminum.

This research attemped to discriminate between subgrain boundary and forest dislocation strengthening at elevated temperatures. This was partially accomplished by observing the dependence of the average subgrain size with steady-state plastic strain in aluminum at high (644 K) temperature. During steady-state the temperature, strain-rate and flow stress are constant and the microstructural feature associated with the rate-controlling process of creep should be fixed.

II. BACKGROUND

A. THEORETICAL

The increase in stress with increase in plastic strain can be described by:

$$\sigma = K\epsilon^m \qquad (2\text{-}1)$$

where σ is the true stress, ϵ is the true strain, and m is the strain hardening exponent. Eventually, a pure metal (and many alloys), that undergoes hardening at elevated temperatures, will reach a steady-state condition where the hardening is balanced by recovery processes.

During the early stage of deformation at elevated temperature, sometimes called Stage I or primary creep (Figure 2.1), the deformation process is dominated by hardening and m is positive. During primary creep the density of randomly arranged (forest) dislocations increases. During this stage many of the dislocations form low energy configurations called subgrain boundaries. These are dislocation tilt or screw boundaries (or mixed) and usually have small ($\simeq 1^o$) misorientations. Eventually, the material reaches a steady-state condition and the strain-rate and flow stress are constant. During steady-state it

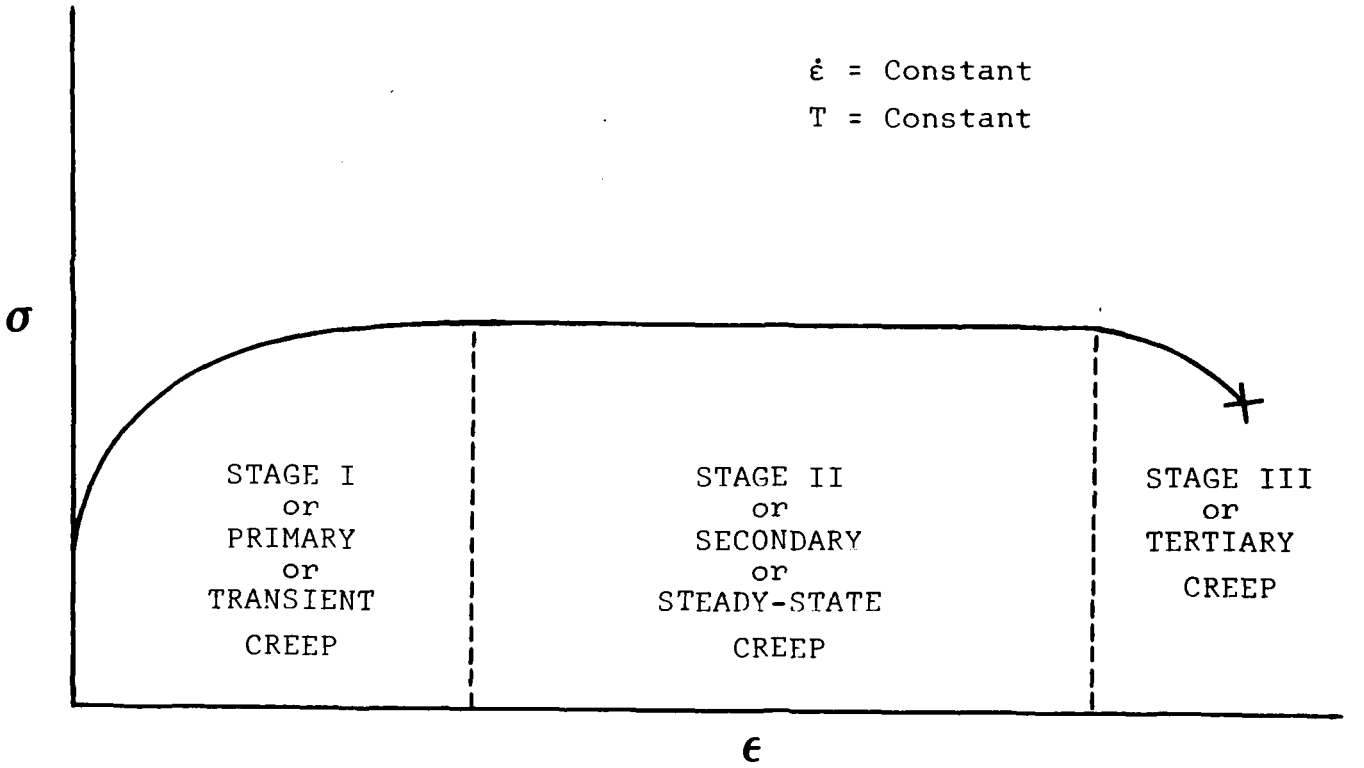

Figure 2.1: Typical elevated-temperature stress versus strain behavior of a pure metal or subgrain-forming alloy.

has been assumed that the dislocation microstructure (λ and ρ) is fixed.

The average (steady-state) subgrain size λ_{ss} can be related to normalized true stress, σ/E, through the equation [Ref. 1]:

$$\lambda_{ss} = k'(\sigma_{ss}/E)^{-1} \tag{2-2}$$

where k' is a constant, σ_{ss} is the steady-state stress and E is the Young's modulus. Also

$$\rho_{ss} = k''(\sigma_{ss}/E) \tag{2-3}$$

where ρ_{ss} is the steady-state forest dislocation density [Ref. 1].

Steady-state conditions are independent of the loading history of the specimen. They are unique to a temperature and strain-rate according to the equation:

$$\dot{\varepsilon}_{ss} = k''' \exp(-Q/RT)(\sigma_{ss}/E)^{n} \tag{2-4}$$

where $\dot{\varepsilon}_{ss}$ is the steady-state strain-rate, k''' is a constant, Q is an activation energy, T is the absolute temperature, and n is the stress exponent. At high temperatures ($T > 0.6T_m$) the activation energy is close to

the value for lattice self-diffusion [Ref. 2], n ≈ 5, and we observe a "power-law". At lower temperatures the activation energy decreases in value. At these same low temperatures, n is not constant and appears to increase in value, and "power-law breakdown" is observed. According to these equations, if, for example, the applied stress is increased or decreased, after a period of transient creep the strain rate, subgrain size, and dislocation density, will approach new values appropriate to the new stress.

Microstructurally, hardening is associated with an increase in randomly arranged (forest) dislocations and a decrease in λ.

B. PREVIOUS WORK

Numerous investigations have attempted to determine wheter ρ or λ is responsible for creep strength. Steady-state structures (data) do not provide clues since there is always a strict relationship between ρ_{ss} and λ_{ss} (Eqs. 2-2 and 2-3). Therefore, most investigations relied on transient creep tests.

Using optical techniques, Ferreira and Stang [Ref. 3] reported that with a stress-decrease, the subgrain size coarsens and converges to the size that would have been attained had the aluminum been deformed originally at the decreased stress level. During this coarsening the strain-rate increased slowly and converged to the steady-state

strain-rate corresponding to the decreased stress level. Because $\dot{\varepsilon}$ and λ changed in tandem, these investigators concluded subgrain strengthening. Because optical (less than very reliable) techniques were utilized, dislocation density changes could not be determined.

Soliman, Ginter, and Mohamed [Ref. 4.], and Young, Robinson, and Sherby [Ref. 5], used TEM to perform experiments similar to those of Ferriera and Stang. They also found that changes in creep-rate, resulting from a stress decrease, correlated with changes in the subgrain size. The dislocation density was not examined.

Kikuchi and Yamaguchi [Ref. 6] performed elevated temperature yield stress tests on aluminum specimens previously deformed to various subgrain sizes and found that the yield stress was again related to changes in λ. The dislocation density was not considered. Calliard and Martin [Ref. 7] concluded, on the basis of <u>in situ</u> creep tests at intermediate temperatures in the high voltage transmission electron microscope (HVEM), that the rate-controlling process for creep is associated with the subgrain boundaries. The forest dislocations were relatively weak obstacles to gliding dislocations.

Langdon, Vastava, and Yavari [Ref. 8] found opposing evidence. They reported that the subgrain size did not change in a stress-decrease test for creep strains as

great as 0.15. They, therefore, concluded forest dislocation strengthening.

Similarly, Parker and Wilshire [Ref. 9] conducted stress reduction experiments to shear strains of 0.005, and found that the subgrain size did not change, despite softening.

Recent work done by Kassner, Ziaai-Moayyed, and Miller [Ref. 10] related the complete dislocation microstructure (λ, ρ) to the yield stress of 304 stainless steel at elevated ($T = 0.6\text{-}0.8\ T_m$) temperatures. It was concluded that forest dislocations provided most of the strength. In subsequent work, Kassner and Elmer [Ref. 11] also examined the dependence of three microstructural features (ρ, λ, and the spacing of dislocations comprising the subgrain boundaries, d) with transient and steady-state creep strain by torsional deformation. Torsion testing allows deformation to much larger strains than tensile deformation. It was found (Figure 2.2) that during steady-state, where $\dot{\varepsilon}$, T, and σ are constant, λ changed while ρ was fixed. This also suggested that ρ rather than λ controlled creep strength. Unfortunately, carbide precipitation and subsequent cavitation at the grain boundaries precluded deformation to strains beyond about one. For this reason the microstructural parameters versus steady-state strain trends were not conclusive.

Stress reduction testing may be ambiguous for constant structure creep testing. Two difficulties may be (a) the

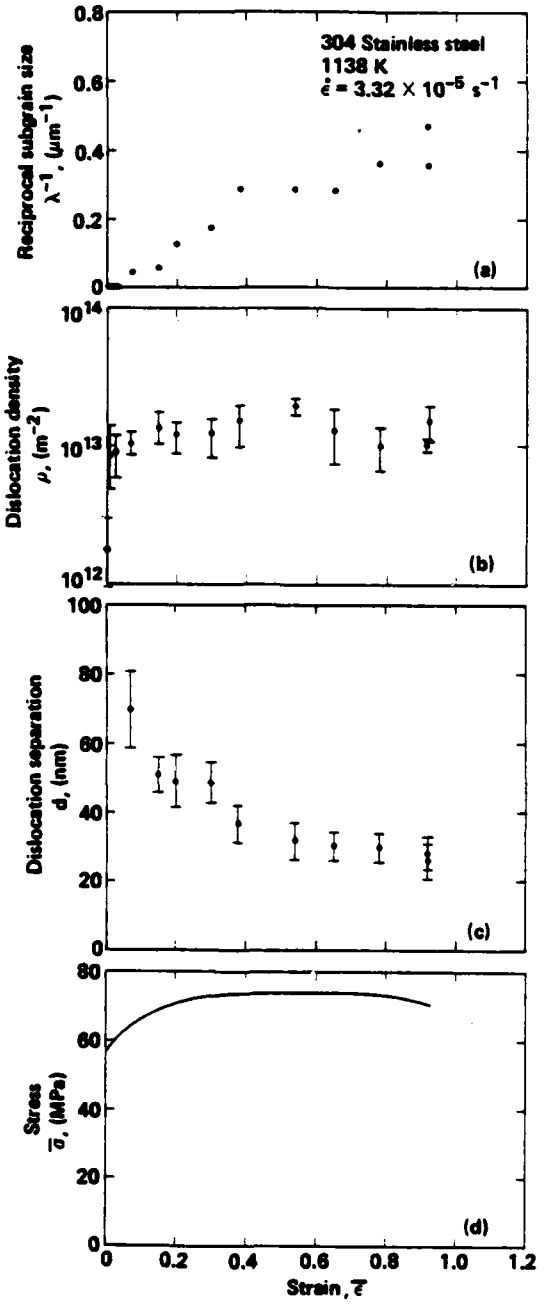

Figure 2.2: Torsional deformation of Type 304 stainless steel at T = 1138 K and $\dot{\epsilon} = 3.32 \times 10^{-5}\ s^{-1}$. (a) reciprocal subgrain size, λ^{-1}, versus strain, ϵ; (b) forest dislocation density, ρ, versus ϵ; (c) subgrain boundary dislocation separation, d, versus ϵ; (d) stress, σ, versus ϵ. [Ref. 11]

inability to accurately measure low transient creep rates after a large stress reduction, and (b) the uncertainty of deciding which creep rate to use after stress reduction, since creep rate recovery is usually a complex interaction of elastic, anelastic, and plastic deformation. The use of steady-state tests such as those of Kassner, et. al., is a possible way to simplify the problem.

The purpose of this thesis was to perform testing analogous to that performed by Kassner and Elmer. Al is a better choice than 304 stainless steel since failure is not expected until very substantial ($\varepsilon > 10$) strains. Therefore, the average subgrain size can be investigated at much larger strains that are well into the steady-state regime.

Past substructural investigations have used either etch pit procedures or transmission electron microscopy (TEM). It was found that the TEM is better since etch pit and other optical techniques may be unreliable [Ref. 12].

The temperature chosen for the present investigation was 644 K (0.69 T_m), a power-law creep temperature (Figure 2.3). Most of the earlier investigations referenced also utilized power-law conditions. Torsion tests were conducted at 644 K to nine different strains (2 transient and 7 steady-state) at a constant strain-rate of 5.04×10^{-4} s^{-1}. The samples were then quenched so as to preserve the elevated

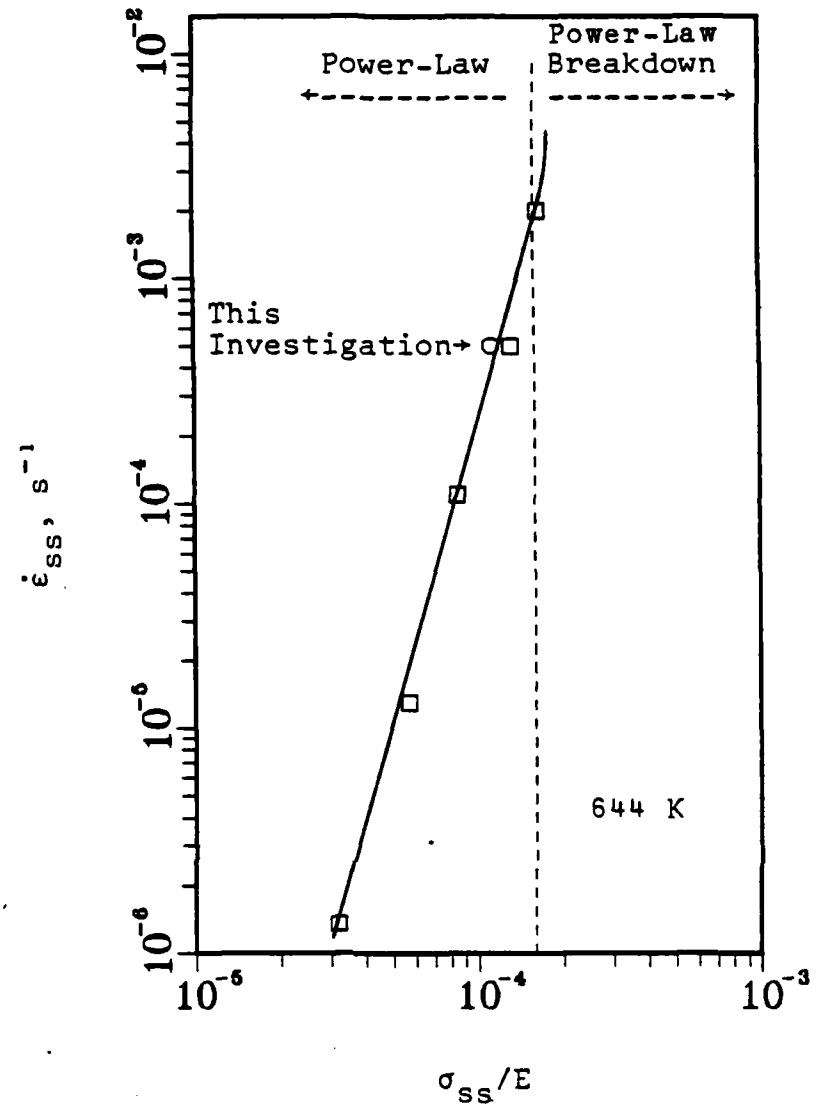

Figure 2.3: Isothermal plots of log(steady-state strain-rate) versus log(modulus compensated steady-state stress). The conditions appropriate to the present study are indicated.

temperature structure. These samples were examined using TEM to observe if changes in the subgrain size had occurred during plastic straining. If the subgrain size changes, then the data would suggest, consistent with recent tests of the same kind on 304 stainless steel and contrary to the general thinking, that subgrain boundaries are probably not associated with the rate-controlling process of creep.

III. EXPERIMENTAL PROCEDURE

A. SPECIMEN TESTING

Figure 3.1 illustrates the high-purity aluminum torsion specimen dimensions. The specimens had a 5.1 mm diameter and a 25.4 mm gage length. Specimens were annealed in vacuum at 698 K for one hour. They were deformed on the Stanford University torsion machine.

The machine is powered by a 10-horsepower electric motor which drives a reduction assembly comprised of two four-speed truck transmissions and two dual chain sprocket assemblies, all coupled in series. This assembly drives a specimen grip which is coupled to the assembly by an electromagnetic clutch. The clutch assembly allows specimen rotation only after the assembly reaches constant speed subsequent to start-up and also allows instantaneous rotation termination upon quenching. The second grip is stationary and connected to a torsional load cell. A quartz tube surrounds the specimen and grips. Through this quartz tube, high purity argon (99.99%) is passed during specimen heating and deformation. The quartz tube has a side arm which connects to a solenoid valve through which water under pressure may pass to provide a quench of the specimen immediately after high temperature deformation. The quench rate has been estimated at 1200 to 1800^{o}C per second

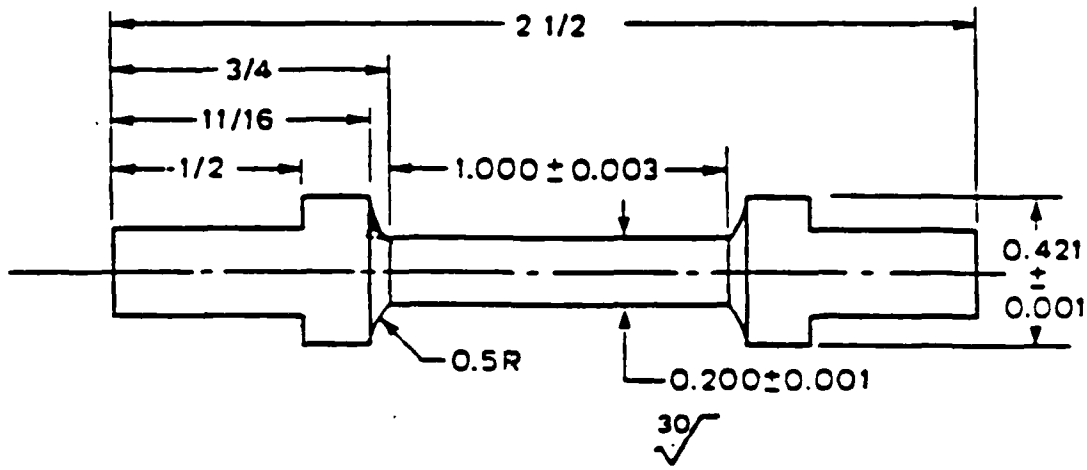

Figure 3.1: Standard dimensions in inches of the torsion specimens used in this investigation.

[Ref. 13]. A dual elliptical radiant furnace provides a rapid heating rate. Nickel foil was wrapped about the external circumference of the quartz tube to provide uniform heating of the specimen and minimize temperature variations within the sample as a function of time. The specimen temperature was maintained at $\pm 3^{o}C$. The specimen ends were coated with BN lubricant so as to reduce the possibility of tensile or compressive stresses in the specimen as a result of slight changes in specimen length during the course of deformation. Torque was measured by using a torsional load cell.

The strain-rate and temperature were held constant at 5.04×10^{-4} s^{-1} and 644 K. Nine torsion specimens were tested from a transient true strain of 0.02 to a true steady-state strain of 16.33.

B. METALLOGRAPHY

Transmission electron microscopy (TEM) foil production was initiated by cutting the torsion specimen transversely. A high-concentration Buehler (.006") wafering blade on a Model 650 Low Speed Diamond Wheel Saw was used for all saw cuts. Since the maximum strain occurs at the outer fiber of a torsion specimen, TEM foils were removed from positions near the surface. Slices parallel to the axis of the specimen (Figure 3.2) were taken such that the maximum thickness of the resulting slab was equal to about one-fourth the specimen diameter.

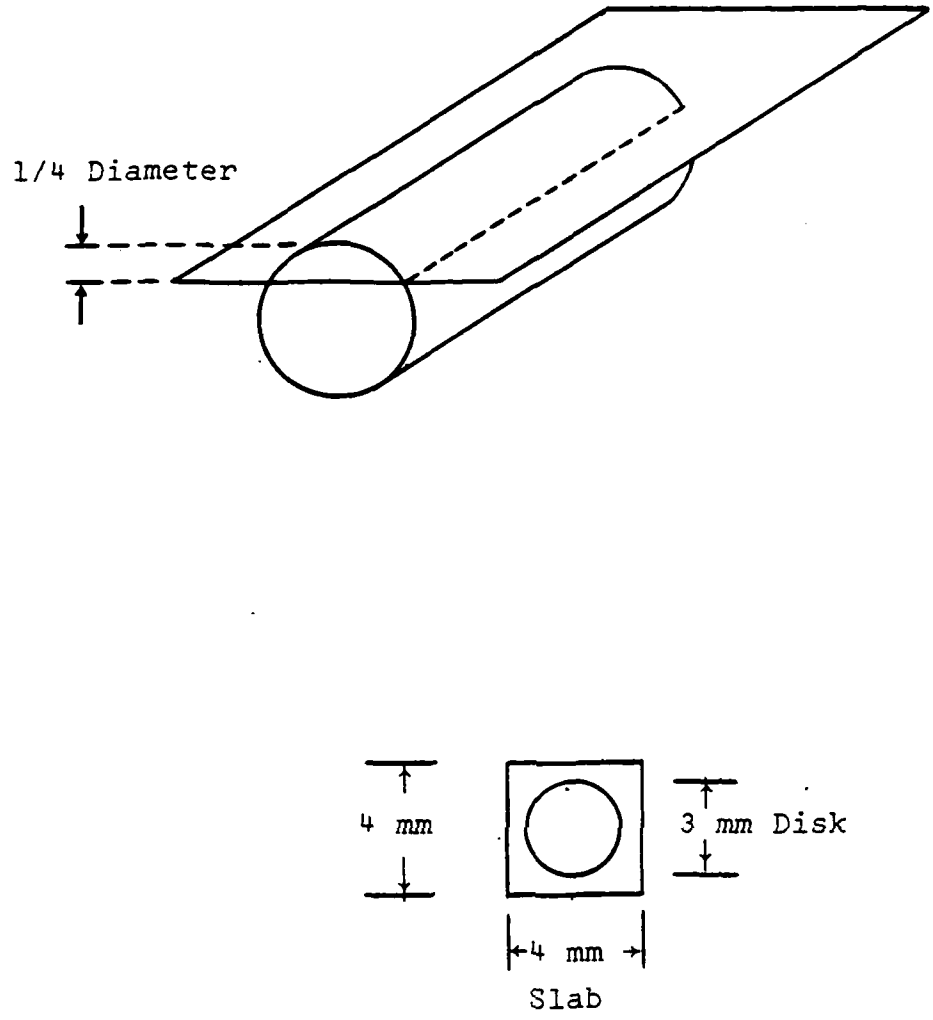

Figure 3.2: Illustration of sectioning of the torsion specimen for TEM thin-foil preparation.

3 mm disks were spark-cut from these slabs (typically 4 mm in length) A Servomet type SMD spark machine (set at HT 6) was used for the extraction. The slabs were mounted on copper trays and brass cutting tubes were utilized.

It was found that grinding annealed Al disks to thicknesses less than 0.45 mm might cause some mechanical damage [Ref. 14]. Therefore, to preserve the creep substructure, grinding below this value was avoided. The disks were hand-ground on 600 grit silicon carbide paper to 0.45 $\pm$0.05 mm thickness. The disks were manufactured into thin foils by electropolishing using a Struers Tenupol 2. The unit was set at 26 volts DC. The electrolyte consisted of 469 parts methyl alcohol, 25 parts sulfuric acid, and 6 parts hydrofluoric acid; it was maintained at approximately $-20^{o}C$. A pump speed setting of 7 was utilized. All foils were examined utilizing a 120 KV JEOL JEM-100CXII Electron Microscope with a 60 degree tilting stage.

The average subgrain size was the quantitative data obtained from the foils. This was determined by photographing (at 2700x) at least 20 random regions from several (usually 4) foils extracted from a given torsion specimen. Kodak 4489 film was used. These photomicrographs were taken at low magnification since a relatively large subgrain size precluded examination at higher magnification. The subgrain sizes were determined by a line intercept

method and the sizes are reported as an average intercept distance.

C. DATA REDUCTION

1. Torsion Analysis

Equivalent uniaxial stress and strain values were converted from torque, and angle of twist measurements by using the following relations [Ref. 15]:

$$\gamma = \frac{\alpha R}{L_o} \tag{3-1}$$

where, γ = shear strain at the full radius position

α = angle of twist

L_o = gage length

R = radial distance to the outer fiber

$$\tau = \frac{M}{2\pi R^3} (3 + n + m') \tag{3-2}$$

where, τ = surface shear stress

M = applied twisting moment

n = strain hardening exponent ($n = 0$ at steady-state)

m' = strain-rate sensitivity exponent

$$\sigma = \sqrt{3}\ \tau \tag{3-3}$$

where, σ = equivalent uniaxial stress, and

$$\epsilon = \gamma/\sqrt{3} \tag{3-4}$$

where, ϵ = equivalent uniaxial strain (the von Mises criterion).

2. Subgrain Size Analysis

The average subgrain size was estimated by placing over several (usually 20) micrographs, random test lines of a total length, ℓ. The number of intersections between the lines and subgrain boundaries N_L allow an estimation of the subgrain size λ by:

$$\lambda = \ell/(N_L M) \tag{3-5}$$

where, λ = average subgrain size, microns

M = negative magnification

N_L = number of subgrain boundary intersections with random test lines

ℓ = length of random test lines (350 mm per micrograph).

IV. RESULTS AND DISCUSSIONS

Nine torsion specimens were deformed to equivalent uniaxial strains of 0.02, 0.1, 0.6, 1.26, 3.11, 4.05, 7.89, 14.3, and 16.33. Two points can be noted from the low magnification photographs of the deformed ($\varepsilon \approx 16.33$) and undeformed torsion specimens in Figure 4.1. First, no dramatic dimensional changes were observed as a consequence of the relatively large deformation. The length changed by less than 0.5 percent. Also, only a small deflection occurred about the axis of rotation despite 45 twists.

Figure 4.2 [Ref. 16] shows the σ versus ε data for high purity Al deforming in tension at temperature/strain-rate conditions ($T = 645$ K, $\dot{\varepsilon} = 19.4 \times 10^{-4}$ s^{-1}) very close to those of the present study. At low loads (as with pure Al deforming at high temperatures) the torsion machine (due to less than perfect alignment of the grips) cannot accurately determine (within 10%) a σ vs. ε curve. However, as indicated by the bracket in the figure, the estimated σ_{ss}, based on Eq. 3-2 ($m' \approx .14$), is in reasonable agreement with the curve.

According to Figure 4.2, steady-state flow is attained after deformation to a uniaxial true strain of approximately 0.15. Therefore, this research only needed to achieve strains substantially beyond 0.15 to attain the goals.

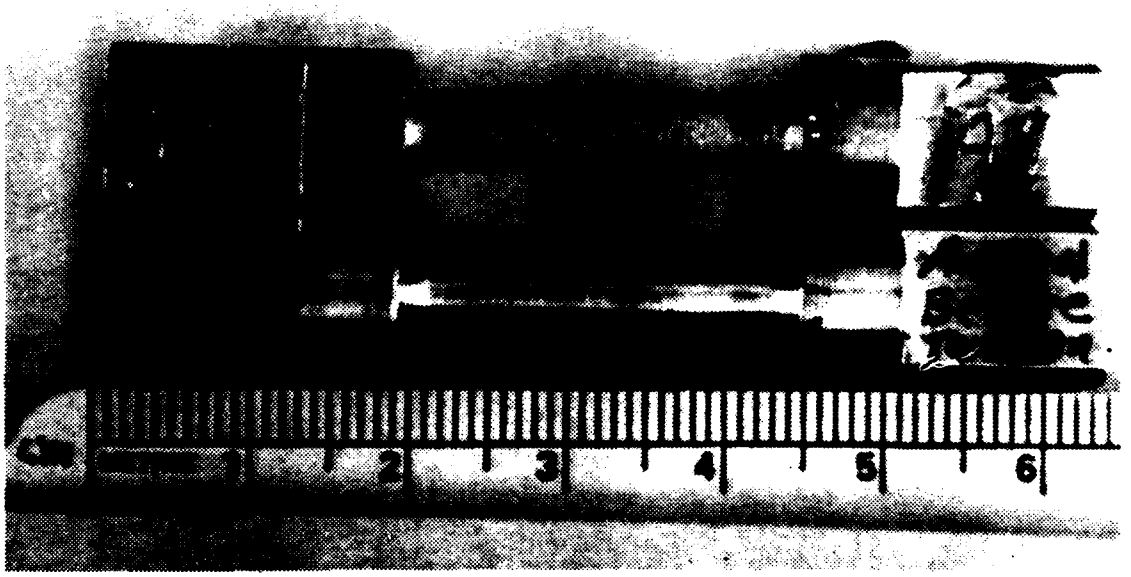

Figure 4.1: A micrograph of a torsion specimen deformed to a strain of 16.33.

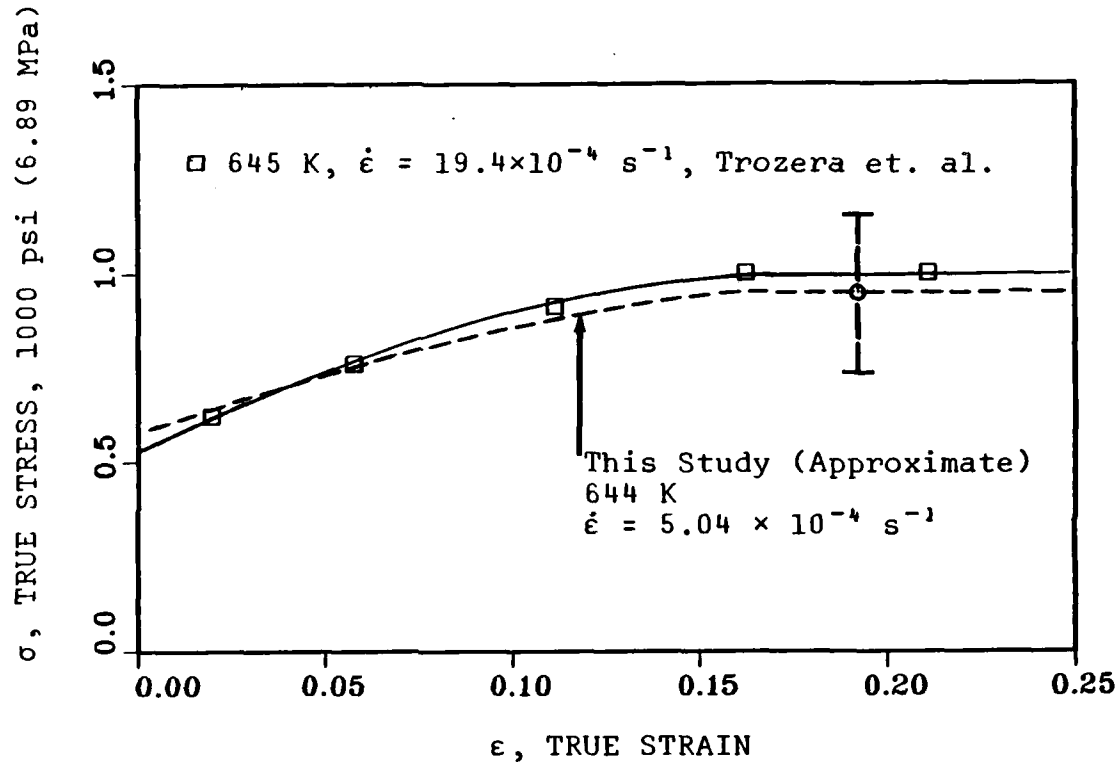

Figure 4.2: The stress versus strain behavior of pure aluminum deformed at 644 K, and a strain rate of 5.04×10^{-4} s^{-1}.

The values of the observed average subgrain size are plotted versus equivalent uniaxial true strain in Figure 4.3. Data per micrograph are detailed in Appendix A. The average subgrain size in the steady-state is approximately 12.5 microns. As shown in Figure 4.4 [Ref. 5] which plots log λ_{ss} versus log (σ_{ss}/E), this value is consistent with other investigations (the modulus of elasticity for Al at 644 K was found to be about 55.5 GN/m^2 [Ref. 16]). The average subgrain size at the transient strain of 0.1 proved to be larger than values found in specimens deformed to steady-state as expected. No subgrain boundaries were found in the specimen deformed to the low transient strain of 0.02, apparently, because the amount of strain hardening was insufficient to generate enough dislocations to form subgrain boundaries (only two foils were examined). It was not always easy to distinguish cellular substructure from subgrains. Subgrains are considered to consist of a very regular arrangement of dislocations, while cells consist of a more diffuse arrangement of dislocations. Only very regular arrangements were considered subgrain boundaries. Ambiguous substructures, however, may have added to data scatter of up to 20%. Ginter, Soliman, and Mohamed reported their accuracy only to be within 16% [Ref. 18].

TEM micrographs of specimens deformed to 14.3 and 16.33 strain at 644 K are illustrated in Figure 4.5. Despite this

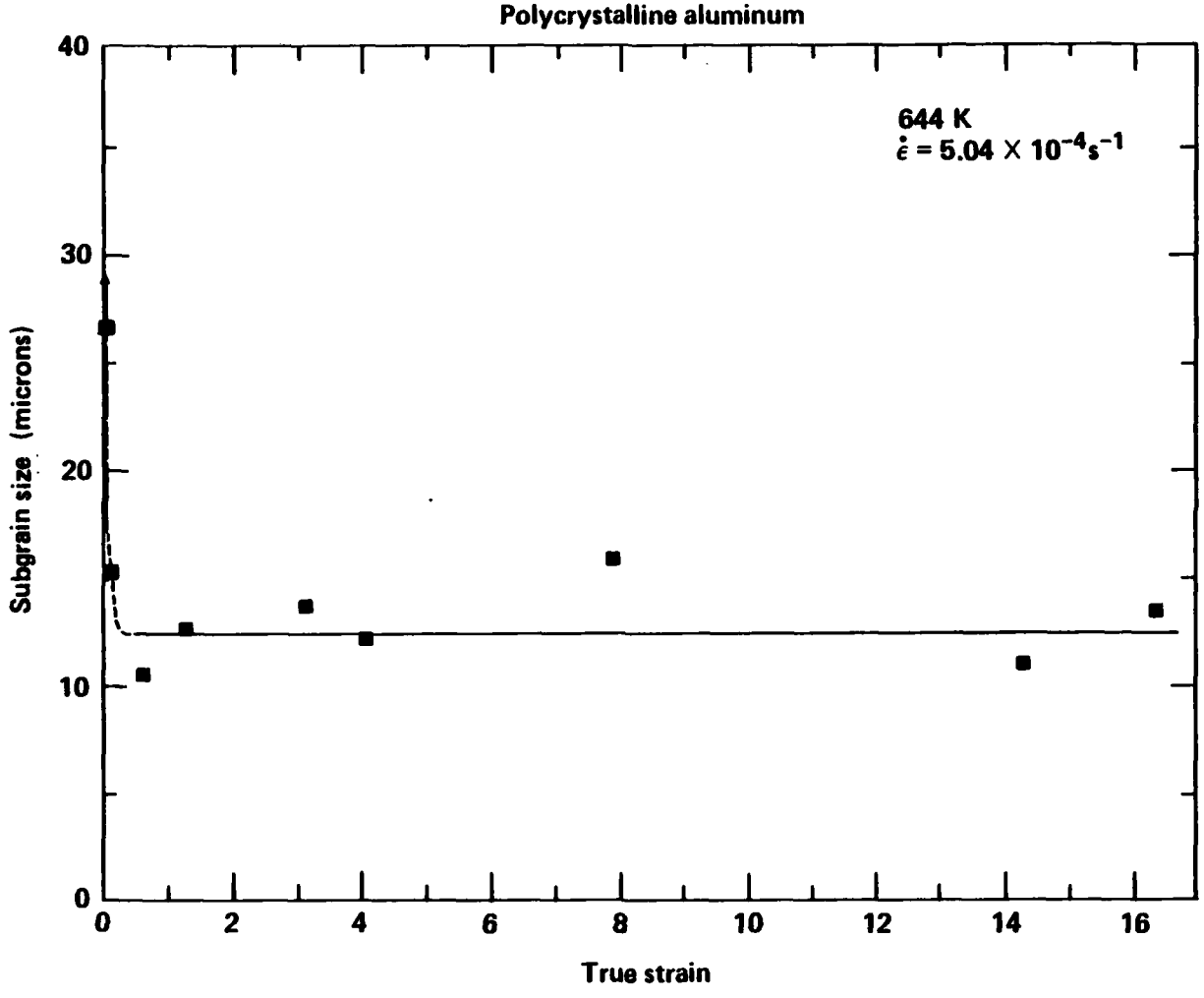

Figure 4.3: λ as a function of ε. λ_{ss} = 12.5 μm ($\sigma_{ss}/E \simeq 1.17 \times 10^{-4}$).

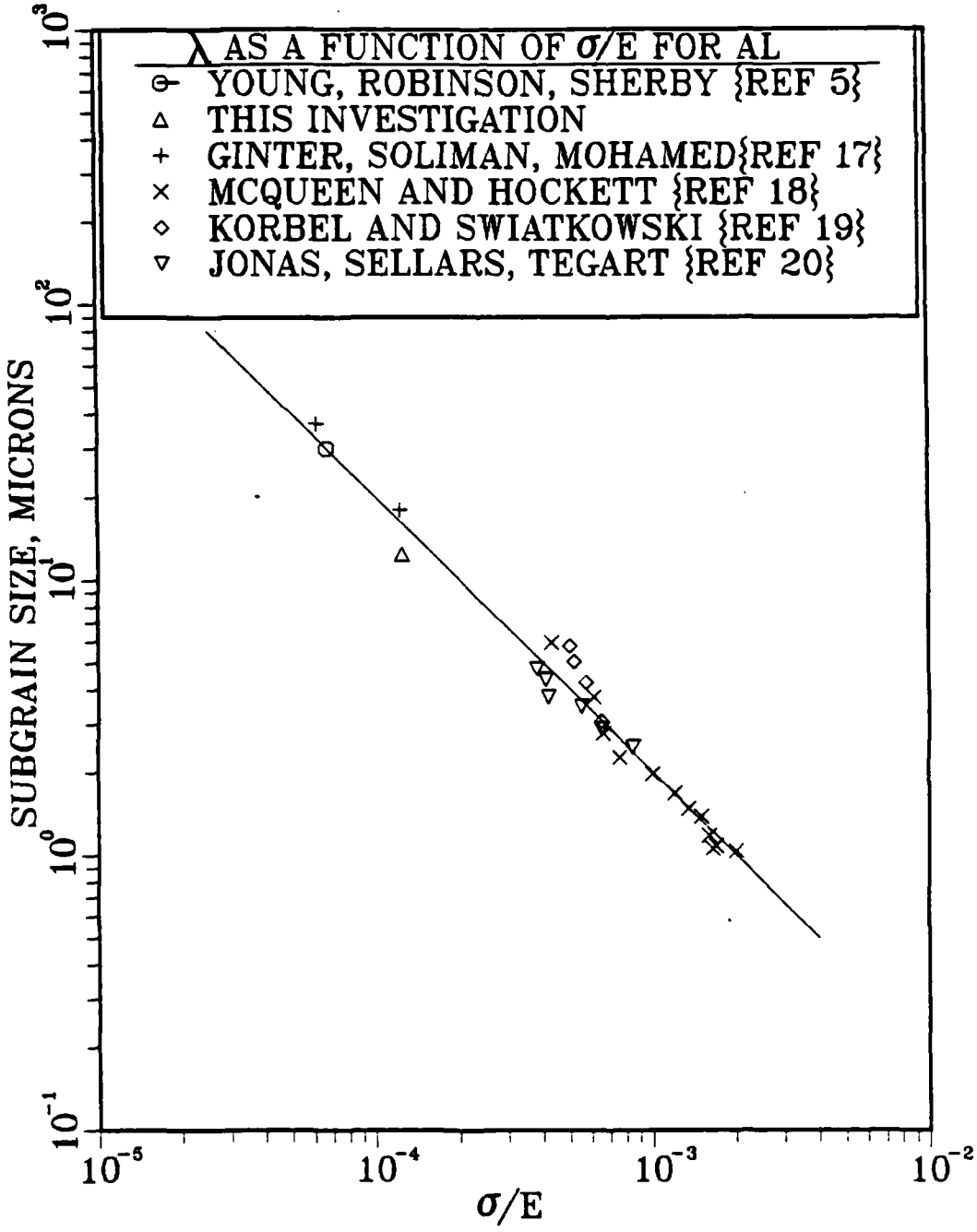

Figure 4.4: The logarithm of the subgrain intercept size, λ_{ss}, as a function of the logarithm of the modulus compensated stress, σ_{ss}/E. All measurements are from transmission electron microscopy.

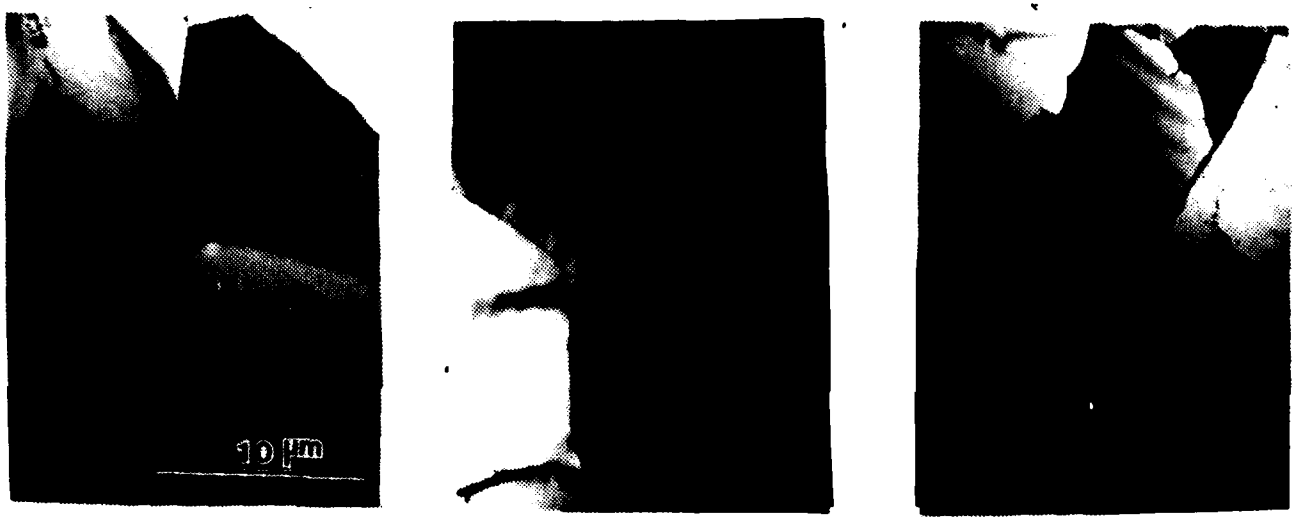

ε = 1430%

ε = 1633%

Al 644 K

Figure 4.5: High purity aluminum TEM micrographs taken from specimens deformed to strains of 14.3 and 16.3 at 644 K. Equiaxed subgrains are observed.

very high level of strain, the subgrains appear equiaxed. In the absence of dynamic recrystallization, the grains (formed by high angle grain boundaries) would evince very heavy distortion (i.e., elongation). Therefore, the micrographs suggest that the subgrain boundaries, once formed, are not permanent and/or are not of a fixed position. A boundary that is formed at early (transient) strains, if fixed, as for the case of high angle boundaries, would evince severe distortion after strains as high as 16. An equiaxed subgrain structure was also observed in the extrusion (large strain) work by Wong, et. al. [Ref. 19]. Therefore, the boundaries must migrate and/or annihilate. This has been suggested earlier by Excell and Warrington [Ref. 20] for Al. The migration has been observed in situ in Al by Calliard and Martin [Ref. 7]. These latter investigators also observed subgrain boundary annihilation in Al. Apparently the formation and annihilation/migration processes are balanced, such that the average subgrain size is fixed during steady-state. However, it is not clear whether this balance is responsible for steady-state conditions. That is, it is not clear whether a constant strain-rate/stress under isothermal conditions is in part a consequence of a constant subgrain size; or whether the rate controlling process for creep is associated with some other feature, i.e., forest dislocations, and that the observation

of a constant subgrain size is the result of a balance of noncontrolling processes.

It is, however, fair to say that the many proponents of theories, in which the rate-controlling process for creep is associated with subgrain boundaries, would consider the observation of a constant subgrain size in this study to be consistent with a subgrain-control theory.

V. CONCLUSIONS AND RECOMMENDATIONS

The following conclusions are drawn from this research: 1) the subgrain size was constant over the very wide range of steady-state strain from about 0.2 to 16 in high purity aluminum deformed at 644 K (0.69 T_m); 2) subgrain boundaries appear to migrate and/or annihilate to maintain an equiaxed appearance.

The following recommendations for further study are made: 1) The determination of the dependence of the misorientation angle between adjacent subgrains with substantial creep strain would be enlightening. Many investigators believe the rate-controlling process is associated with subgrain boundaries and that the strain-rate or strength is dependent on the spacing of dislocations in the boundary. There is preliminary evidence that in Al, the spacing actually decreases during steady-state. If the spacing changes during steady-state, this feature may not be an important variable. 2) The determination of the dependence of forest dislocation density with strain would also be interesting. In particular, it is worth determining whether the forest dislocation density versus strain trends are consistent with earlier experiments by Kassner, et. al. [Ref. 11]

Hopefully, with enough data, the important microstructural features can be identified. Then the existing creep theories could be evaluated and possibly modified so as to be consistent with the data.

LIST OF REFERENCES

1. Mukherjee, A. K., "High Temperature Creep," Treatise on Materials Science and Technology, R. J. Arsenault, ed., Academic Press, Vol. 6, p. 163, 1975.

2. Sherby, O. D. and Burke, P. M., "Mechanical Behavior of Crystalline Solids at Elevated Temperature," Progess in Materials Science, Vol. 13, p. 325, 1967.

3. Ferreira, I., and Stang, R. G., "The Effect of Stress and Subgrain Size on the Creep Behavior of High Purity Aluminum," Acta Metallurgica, Vol. 31, p. 585, 1983.

4. Soliman, M. S., Ginter, T. J., and Mohamed, F. A., "An Investigation of the Stress Exponent and Subgrain Size in Al After Stress Reduction," Philosophical Magazine A, Vol. 48, No. 1, p. 73, 1983.

5. Young, C. M., Robinson, S. L., and Sherby, O. D., "Effect of Subgrain Size on the High Temperature Strength of Polycrystalline Aluminum as Determined by Constant Strain Rate Tests," Acta Metallurgica, Vol. 23, p. 633, May 1975.

6. Kikuchi, S. and Yamaguchi, A., "Effects of Prestrain at High Temperatures on the Strength of Aluminum," Strength of Metals and Alloys, H. J. McQueen, ed., Pergamon Press, p. 899, 1985.

7. Calliard and Martin, "Microstructure of Aluminum During Creep at Intermediate Temperature-II, In Situ Study of Subboundary Properties," Acta Metallurgica, Vol. 30, p. 791, 1982.

8. Langdon, T. G., Vastava, R. B., and Yavari, P., Strength of Metals and Alloys, P. Hassen, V. Gerold and G. Kostorz, eds., Pergamon Press, p. 271, 1979.

9. Parker, J. D., and Wilshire, B., "On the Subgrain Size Dependence of Creep," Philosophical Magazine, Vol. 34, p. 485, 1976.

10. Kassner, M. E., Ziaai-Moayyed, A. A., and Miller, A. K., "Some Trends Observed in the Elevated-Temperature Kinematic and Isotropic Hardening of Type 304 Stainless Steel," Metallurgical Transactions A, Vol. 16A, p. 1069, 1985.

11. Kassner, M. E., and Elmer, J. W., "Variation in the Spacing of Dislocations in Subgrain Boundaries with Creep Strain in Type 304 Stainless Steel," Strength of Metals and Alloys, H. J. Queen, ed., Pergamon Press, p. 953, 1985.

12. Ginter, T. J., and Mohamed, F. A., "The Stress Dependence of the Subgrain Size in Aluminum," Journal of Materials Science, Vol. 17, p. 2007, 1982.

13. Young, C. M., Cady, E. M., and Sherby, O. D., Studies on the Warm Working Characteristics of Alloys, U.S. Army Materials and Mechanical Research Center, Watertown, MA, Report CTR-72-27, 1972.

14. Kassner, M. E. and Echer, C. J., Mechanical Damage Introduced into Aluminum Monocrystals during TEM Thin-foil Preparation, Lawrence Livermore National Laboratory, Report UCRL-92712, May 1985.

15. Kassner, M. E., The Separate Roles of Forest Dislocations and Subgrains in the Isotropic Hardening of Type 304 Stainless Steel, Ph.D. Thesis, Stanford University, Stanford, California, March 1981.

16. Trozera, T. A., Sherby, O. D., and Dorn, J. E., "Effect of Strain Rate and Temperature on the Plastic Deformation of High Purity Aluminum," Trans ASM, Vol. 49, p. 173, 1957.

17. Ginter, T. J., Soliman, M. S., and Mohamed, F. A., "Effect of Creep Substructure on the Stress Exponent of Al Following Stress Reductions," Philosophical Magazine A, Vol. 50, p. 9, 1984.

18. McQueen, H. J. and Hockett, J. E., "Microstructures of Aluminum Compressed at Various Rates and Temperatures," Metallurgical Transactions A, Vol. 1, p. 2997, 1970.

19. Korbel, A. and Swiatkowski, K., "Role of Strain Rate in the Formation of Dislocation Structure and Its Influence on the Mechanical Properties of Aluminum," Metal Science Journal, Vol. 6, p. 60, 1972.

20. Jonas, J. J., Sellars, C. M., and Tegart, W. J., "Strength and Structure under Hot-working Conditions," Metallurgical Reviews, Vol. 14, p. 1, 1969.

21. Mondolfo, L. F., Aluminum Alloys: Structure and Properties, Butterworths, London, p. 82, 1976.

22. Wong, W. A., McQueen, H. J., and Jonas, J. J., "Recovery and Recrystallization of Aluminum during Extrusion," The Journal of the Institute of Metals, Vol. 95, p. 129, 1967.

23. Excell, S. F., and Warrington, D. M., "Subgrain Boundary Migration in Aluminum," Philosophical Magazine, Vol. 26, p. 1121, 1972.

APPENDIX A: DATA

TABLE A.1

Specimen A-1, $\varepsilon = 3.11$, $T = 644$ K, $\dot{\varepsilon} = 5.04 \times 10^{-4} s^{-1}$, $\lambda_{AVE} = 13.8$ μm

Foil No.	Micrograph No.	Magnification	No. Intercepts for 350 mm of Random Lines
A-1,1	3430	2700x	16
A-1,1	3431	2700x	10
A-1,1	3432	2700x	9
A-1,1	3433	2700x	13
A-1,1	3434	2700x	11
A-1,1	3435	2700x	12
A-1,3	3393	2700x	8
A-1,3	3394	2700x	4
A-1,3	3395	2700x	10
A-1,3	3396	2700x	4
A-1,3	3397	2700x	14
A-1,3	3398	2700x	21
A-1,3	3399	2700x	7
A-1,3	3400	2700x	9
A-1,3	3401	2700x	4
A-1,3	3402	2700x	5
A-1,8	3424	2700x	8
A-1,8	3425	2700x	6
A-1,8	3426	2700x	7
A-1,8	3427	2700x	11
A-1,8	3428	2700x	12
A-1,8	3429	2700x	6
A-1,9	3480	2700x	9

TABLE A.2

Specimen A-3, $\varepsilon = 0.60$, $T = 644$ K, $\dot{\varepsilon} = 5.04 \times 10^{-4} s^{-1}$, $\lambda_{AVE} = 10.57$ μm

Foil No.	Micrograph No.	Magnification	No. Intercepts for 350 mm of Random Lines
A-3,2	3470	2700x	14
A-3,2	3471	2700x	6
A-3,2	3472	2700x	27
A-3,2	3473	2700x	3
A-3,2	3474	2700x	10
A-3,2	3475	2700x	11
A-3,2	3476	2700x	14
A-3,2	3477	2700x	13
A-3,9	3464	2700x	7
A-3,9	3465	2700x	10
A-3,9	3466	2700x	15
A-3,9	3467	2700x	10
A-3,9	3468	2700x	13
A-3,10	3479	2700x	20
A-3,11	3469	2700x	11

TABLE A.3

Specimen A-4, $\varepsilon = 1.26$, $T = 644$ K, $\dot{\varepsilon} = 5.04 \times 10^{-4} s^{-1}$, $\lambda_{AVE} = 12.6$ μm

Foil No.	Micrograph No.	Magnification	No. Intercepts for 350 mm of Random Lines
A-4,2	3412	2700x	9
A-4,2	3413	2700x	15
A-4,2	3414	2700x	3
A-4,2	3415	2700x	10
A-4,2	3416	2700x	13
A-4,2	3417	2700x	5
A-4,3	3403	2700x	9
A-4,3	3404	2700x	14
A-4,3	3405	2700x	12
A-4,3	3406	2700x	13
A-4,3	3407	2700x	12
A-4,3	3408	2700x	9
A-4,3	3409	2700x	7
A-4,3	3410	2700x	5
A-4,3	3411	2700x	10
A-4,4	3364	2700x	14
A-4,4	3365	2700x	10
A-4,4	3366	2700x	21
A-4,4	3367	2700x	4
A-4,4	3368	2700x	9
A-4,4	3369	2700x	11
A-4,6	3370	2700x	16
A-4,6	3371	2700x	10
A-4,6	3372	2700x	6

TABLE A.4

Specimen A-5, ϵ = 4.05, T = 644 K, $\dot{\epsilon} = 5.04 \times 10^{-4} s^{-1}$, λ_{AVE} = 12.3 μm

Foil No.	Micrograph No.	Magnification	No. Intercepts for 350 mm of Random Lines
A-5,2	3356	2700x	7
A-5,2	3357	2700x	5
A-5,3	3358	2700x	17
A-5,3	3359	2700x	9
A-5,3	3360	2700x	5
A-5,3	3361	2700x	22
A-5,3	3362	2700x	1
A-5,3	3363	2700x	15
A-5,8	3338	2700x	10
A-5,8	3339	2700x	13
A-5,8	3340	2700x	8
A-5,8	3341	2700x	6
A-5,8	3342	2700x	0
A-5,8	3343	2700x	1
A-5,8	3344	2700x	18
A-5,8	3345	2700x	8
A-5,8	3346	2700x	8
A-5,11	3347	2700x	24
A-5,11	3348	2700x	10
A-5,11	3349	2700x	14
A-5,11	3350	2700x	14
A-5,11	3351	2700x	7
A-5,11	3352	2700x	20
A-5,11	3353	2700x	6
A-5,11	3354	2700x	14
A-5,11	3355	2700x	12

TABLE A.5

Specimen A-6, ϵ = 0.10, T = 644 K, $\dot{\epsilon}$ = $5.04 \times 10^{-4} s^{-1}$, λ_{AVE} = 15.35 μm

Foil No.	Micrograph No.	Magnification	No. Intercepts for 350 mm of Random Lines
A-6,1	3436	2700x	6
A-6,1	3437	2700x	13
A-6,1	3438	2700x	7
A-6,1	3439	2700x	10
A-6,1	3440	2700x	17
A-6,1	3441	2700x	12
A-6,1	3442	2700x	8
A-6,2	3517	2700x	4
A-6,2	3518	2700x	5
A-6,2	3519	2700x	7
A-6,2	3520	2700x	5
A-6,2	3521	2700x	3
A-6,11	3526	2700x	11
A-6,11	3527	2700x	6
A-6,11	3528	2700x	16
A-6,11	3529	2700x	11
A-6,11	3530	2700x	15
A-6,12	3511	2700x	13
A-6,12	3512	2700x	15
A-6,12	3513	2700x	3
A-6,12	3514	2700x	6
A-6,12	3515	2700x	12
A-6,12	3516	2700x	11
A-6,15	3522	2700x	3
A-6,15	3523	2700x	0
A-6,15	3524	2700x	0
A-6,15	3525	2700x	9

TABLE A.6

Specimen A-7, $\varepsilon = 7.89$, T = 644 K, $\dot{\varepsilon} = 5.04 \times 10^{-4} s^{-1}$, $\lambda_{AVE} = 15.92$ μm

Foil No.	Micrograph No.	Magnification	No. Intercepts for 350 mm of Random Lines
A-7,1	3448	2700x	13
A-7,1	3449	2700x	11
A-7,1	3450	2700x	8
A-7,3	3451	2700x	8
A-7,3	3452	2700x	8
A-7,3	3453	2700x	5
A-7,3	3454	2700x	8
A-7,3	3455	2700x	10
A-7,5	3457	2700x	19
A-7,5	3458	2700x	9
A-7,5	3459	2700x	8
A-7,5	3460	2700x	8
A-7,5	3461	2700x	6
A-7,5	3462	2700x	1
A-7,5	3463	2700x	10
A-7,6	3418	2700x	5
A-7,6	3419	2700x	10
A-7,6	3420	2700x	5
A-7,6	3421	2700x	4
A-7,6	3422	2700x	6
A-7,6	3423	2700x	9

TABLE A.7

Specimen A-8, ε = 14.3, T = 644 K, $\dot{\varepsilon} = 5.04 \times 10^{-4} s^{-1}$, λ_{AVE} = 10.98 μm

Foil No.	Micrograph No.	Magnification	No. Intercepts for 350 mm of Random Lines
A-8,9	3483	2700x	14
A-8,9	3484	2700x	7
A-8,9	3485	2700x	7
A-8,9	3486	2700x	15
A-8,9	3487	2700x	17
A-8,10	3501	2700x	21
A-8,10	3502	2700x	13
A-8,10	3503	2700x	10
A-8,10	3504	2700x	10
A-8,10	3505	2700x	9
A-8,10	3506	2700x	15
A-8,10	3507	2700x	13
A-8,10	3508	2700x	10
A-8,10	3509	2700x	16
A-8,10	3510	2700x	9
A-8,11	3492	2700x	15
A-8,11	3493	2700x	12
A-8,11	3494	2700x	11
A-8,11	3495	2700x	11
A-8,11	3496	2700x	9
A-8,11	3498	2700x	13
-8,11	3499	2700x	13
A-8,12	3488	2700x	11
A-8,12	3489	2700x	9
A-8,12	3490	2700x	7
A-8,12	3491	2700x	10

TABLE A.8

Specimen A-9, ϵ = 16.33, T = 644 K, $\dot{\epsilon} = 5.04 \times 10^{-4} s^{-1}$, λ_{AVE} = 13.47 μm

Foil No.	Micrograph No.	Magnification	No. Intercepts for 350 mm of Random Lines
A-9,1	3531	2700x	9
A-9,1	3532	2700x	13
A-9,1	3534	2700x	10
A-9,1	3535	2700x	12
A-9,1	3536	2700x	2
A-9,1	3537	2700x	9
A-9,3	3482	2700x	8
A-9,3	3545	2700x	8
A-9,3	3546	2700x	10
A-9,3	3547	2700x	11
A-9,3	3548	2700x	9
A-9,3	3549	2700x	9
A-9,3	3550	2700x	11
A-9,3	3551	2700x	10
A-9,3	3552	2700x	13
A-9,4	3553	2700x	9
A-9,4	3554	2700x	8
A-9,4	3555	2700x	0
A-9,4	3556	2700x	12
A-9,4	3560	2700x	13
A-9,4	3561	2700x	10
A-9,4	3562	2700x	11
A-9,8	3538	2700x	12
A-9,8	3539	2700x	6
A-9,8	3540	2700x	12
A-9,8	3541	2700x	11
A-9,8	3542	2700x	9
A-9,8	3543	2700x	12

TABLE A.8 (CONTINUED)

Foil No.	Micrograph No.	Magnification	No. Intercepts for 350 mm of Random Lines
A-9,9	3543	2700x	12
A-9,9	3481	2700x	10

TABLE A.9

Specimen A-10, $\varepsilon = 0.02$, T = 644 K, $\dot{\varepsilon} = 5.04 \times 10^{-4} s^{-1}$, $\lambda_{AVE} = \infty$ μm

Foil No.	Micrograph No.	Magnification	No. Intercepts for 350 mm of Random Lines
A-10,1	(TEN REGIONS)	2700X	0
A-10,3	(TEN REGIONS)	2700X	0

INITIAL DISTRIBUTION LIST

		No. Copies
1.	Defense Technical Information Center Cameron Station Alexandria, Virginia 22304-6145	2
2.	Library, Code 0142 Naval Postgraduate School Monterey, California 93943-5100	2
3.	Department Chairman, Code 69Mx Department of Mechanical Engineering Naval Postgraduate School Monterey, California 93943-5100	1
4.	Professor M. E. Kassner, Code 69 Department of Mechanical Engineering Naval Postgraduate School Monterey, California 93943-5100	5
5.	Commanding Officer, Code 330 Attn: LT Paul P. Mieszczanski Philadelphia Naval Shipyard Philadelphia, Pennsylvania 19112-5087	5

END

FILMED

12-85

DTIC